SAND2011-5743C

TROUGH HEAT COLLECTION ELEMENT DEFORMATION AND SOLAR INTERCEPT IMPACT

Brian D. Iverson, Scott M. Flueckiger and Brian D. Ehrhart

Concentrating Solar Technologies Dept., Sandia National Laboratories, PO Box 5800, Albuquerque, NM, 87185-1127, USA

+1 (505) 844-0480, bdivers@sandia.gov

1. Introduction

As efforts continue to reduce costs for parabolic trough based concentrating solar power, the use of a thermal storage salt as the working fluid has received increased attention. The interest in using a molten salt as the heat transfer fluid is driven by a number of reasons. First, it allows the incorporation of a thermal storage medium directly in the plant and eliminates an intermediate heat exchanger common to indirect storage systems. This inclusion of storage provides the avenue for an increase in capacity factor and plant availability. Second, molten salt formulations have a higher maximum operating temperature than the commonly used oils. This raise in temperature and corresponding increase in overall temperature difference enables the power block to produce more power and at a higher efficiency [1].

Inclusion of storage and higher operating temperatures with their associated benefits result in a reduction of levelized cost of energy making energy production by solar means more attractive. Application of salt in a trough plant operation has been inaugurated most notably in the Archimede plant by ENEA/ENEL in Priolo Gargallo, Italy [2]. However, concerns exist regarding the use of molten salt in trough collectors including the potential of salt solidification and recovery from freezing in the event of total power failure. Lower melting point salt formulations have been developed that would essentially provide increased time before the initiation of solidification [3, 4]. Delay of the onset of freezing can be effective assuming a timely power restoration and essentially mitigates the risk of such a solidification event occurring. Regardless, any salt that has a solidification temperature above ambient temperature would still have some level of risk in its usage.

The potential for a freeze event necessitates an understanding of freeze event recovery and the possible detrimental effects associated with returning to normal operation. To this end, Sandia National Laboratories has constructed a test facility to expose trough heat collection elements to conditions experienced during solidification and melting cycles. Early experiments indicated the possibility of tube deformation and initiated a series of studies to quantify and characterize the bending behavior [5]. In an effort to model the system and stress imparted by the expanding salt, studies were performed to obtain mechanical and thermal properties for three salt formulations (with melting temperatures from 90-220 °C) in the solid-phase [6, 7]. These works included results for unconfined compressive strength, indirect tensile strength, Young's modulus, Poisson's ratio, coefficient of thermal expansion, thermal conductivity and specific heat. The current work seeks to quantify the risk and the conditions associated with tube deformation by quantifying deflection under multiple conditions and calculating the impact on solar intercept through ray tracing.

2. Experimental Facility

Figure 1 illustrates the test facility constructed at Sandia National Laboratories for performing solidification/melt cycling on receiver tubes. The mounting system mimics the LS-2 trough design with comparable moment arms to allow axial expansion of trough receiver tubes with change in temperature (see Figure 1 for dimensions). The ~4 m absorber is constrained with two collars (4.27 m apart) fixed near the risers, connecting to bracket arms attached to the ground. The east bracket is fixed in the vertical direction at the base while the west bracket is free to rotate at two pin joints. Impedance heating circuitry and equipment has been included in the facility as a means to preheat/heat the receiver tube and is capable of providing an output of 4.25, 5.1, 5.9, 6.8, 7.6, or 8.5 volts up to 9 kVA. Standpipes at either end of the receiver tube mimic the orientation of the flex hoses at the end of a solar collector assembly when modules are in a stow position. These standpipes are heavily insulated with multiple wraps of Superwool Plus (8 lb).

Thermocouples (at positions indicated in Figure 1) monitor temperature throughout a test cycle. As the internal thermocouples are cantilevered from their entry point in the standpipe, their radial position is not guaranteed. Tube position is measured relative to the glass enclosure and compared to its initial position to determine deformation change using an optical measurement tool with digital images [8]. A video camera also records position (once every 90 s) at the center of the tube length to visually monitor tube deflection with time.

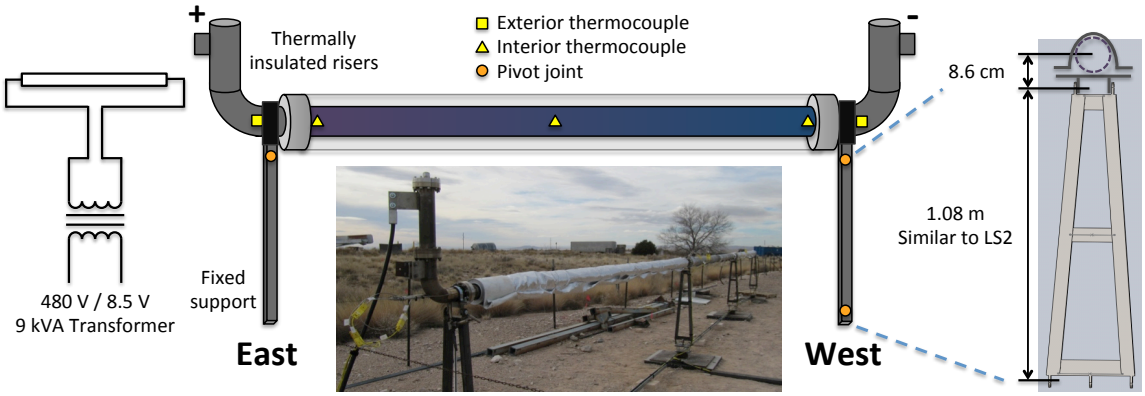

Figure 1. Depiction of the test facility for solidification/melt cycles on trough heat collection elements.

3. Empty Tube

Deflection analysis of the Schott PTR70 absorber tube began with a baseline case of an empty tube exposed to direct sunlight. Experimental investigation followed the thermal and optical methods outlined above. A numerical simulation of this scenario was composed of two distinct models, thermal and structural, and validated with experimental data. The thermal model simulates the transient response of the absorber tube exposed to direct sunlight. Temperature fields at discrete time points are then imported into the structural model to calculate the resultant deflection due to thermal expansion. While the glass cover is excluded from the model geometry, the thermal influence is replicated with boundary conditions discussed below. Assuming solar altitude effects to be negligible, a vertical symmetry plane is defined through the middle of the tube assembly along the east-west axis.

Thermal Model

Prior to exposure to direct sunlight, the experimental test setup (and corresponding models) begin at a uniform initial temperature of 9 °C. The heat flux incident on the absorber surface is derived from the direct normal insolation (DNI) measurements associated with the test setup. For a test performed on April 27, 2011 from 11:00 am to 3:00 pm MST, the average incident DNI was 1065 W/m^2. The actual flux received by the absorber tube is reduced by both the surface solar absorptivity (0.95) and varies with circumferential position (cosine loss), which generates a non-uniform heat flux along the upper half of the absorber. To simulate this phenomenon, the incident heat flux profile is divided into three, 30° intervals (Figure 2a). From vertical to 30°, the model absorber receives a heat flux of 966.2 W/m^2; from 30° to 60 °, the incident flux is 707.3 W/m^2; and from 60° to 90° the flux is 258.9 W/m^2. The total flux incident on the tube is equal to the integration of these regions. The extent of these fluxes is limited to the length of the glass cover, approximately 3.91 m. In addition to heating from incident sunlight, a portion of received energy is rejected to the colder surroundings. The loss per unit length associated with this heat rejection (within ±10 W/m) for a Schott PTR70 absorber was modeled by Burkholder and Kutscher as a function of the absorber temperature, T_{abs} [9].

$$q' = 0.141 T_{abs} + 6.48 \times 10^{-9} T_{abs}^4 \quad (1)$$

For a measured ambient temperature of 14 °C, this function is well simulated by an absorber emissivity of 0.06 (see also [9]) and a convection coefficient of 0.05 W/m^2·K. Heat loss in the standpipe and mounting

regions are simulated with a 5 W/m^2·K convection coefficient. Thermal transport across pin joints in the brackets is neglected as the convective losses in the standpipe account for any transport through the bracket arms and collars. Radiation exchange inside the empty absorber tube is simulated as a blackbody.

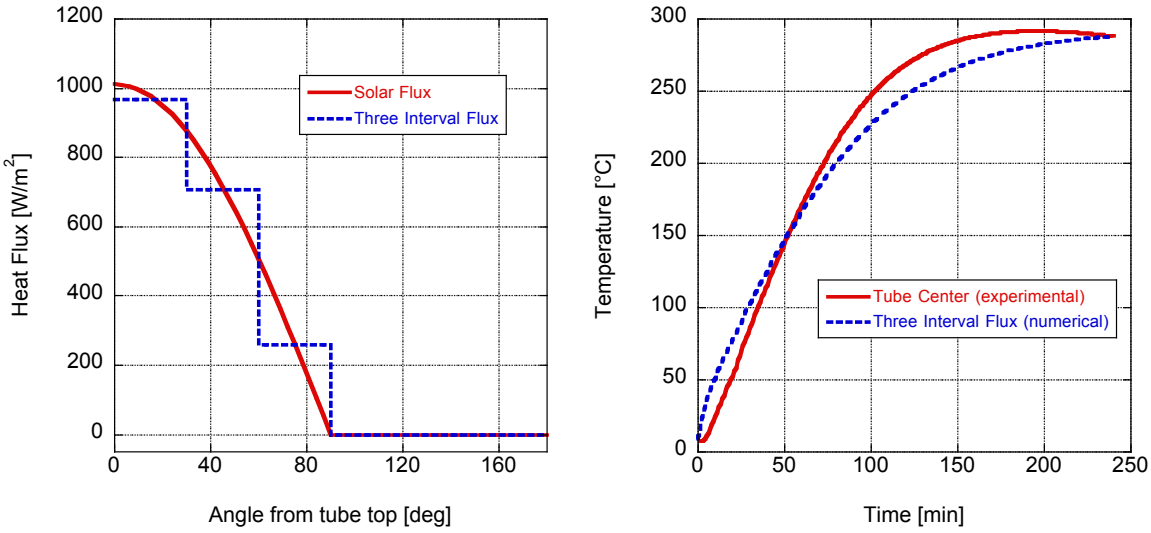

(a) (b)

Figure 2. (a) Simulated incident heat flux along the absorber tube surface. (b) Experimental and simulated temperature response of empty absorber tube with sun heating. Thermocouple location is inside the absorber tube at the lengthwise midpoint; numerical model temperature location is the top, center of the tube.

The thermal solution is calculated with ANSYS 13.0 Workbench [10], a commercial finite-element solver. The model geometry is meshed with 51161 elements (reducing the element count yields identical results). The temperature response at the midpoint of the absorber tube is plotted in Figure 2b along with thermocouple data measured inside the center of the tube. The two data sets show a similar temperature response in time with a final numerical convergence to 288 °C at the top of the tube in the center of the length. Disparity between the thermocouple and model during the heating process may be attributed to position uncertainty of the thermocouple inside the absorber. Due to the circumferentially varying heat flux, the bottom of the absorber converges to a lower temperature of 276 °C.

Structural Model

With a higher temperature along the tube top relative to the bottom, the absorber tube bends upward due to the disparity in thermal expansion. The maximum vertical deflection is calculated from the solved temperature field using both analytical and numerical models.

First, we introduce the analytical approach. The change in length at both the top and bottom of the absorber tube is known from the coefficient of thermal expansion of the absorber material (stainless steel 321H). To simplify the calculation, the top and bottom temperatures are assumed constant along the length of the tube. From the results of the thermal simulation, this approximation is appropriate for the tube region inside the glass cover. The disparity in expansion is solved with the following equation, where the cold receiver length inside the glass cover $L_{abs,0}$ is 3.91 m.

$$L_{top} - L_{bot} = L_{abs,0} \cdot \alpha \cdot \left(T_{top} - T_{bot}\right) \tag{1}$$

Approximating the resultant deformation as parabolic, a second-order equation is fit to the deflection and solved for the maximum vertical deflection. Three boundary conditions are required to construct a parabolic fit to the profile. First, the slope at the ends of the tube (parabola) is solved from trigonometry and equal to half the disparity in length between the tube top and bottom divided by the tube diameter. Second, the slope

at the point of maximum deflection (assumed to be the midpoint) is zero. Third, the horizontal length between the east-west ends of the parabola is assumed to be equal to the nominal receiver length. The second-order fit is then fully defined and solved for the vertical deflection following,

$$y_{\max} = \frac{\left(L_{top} - L_{bot}\right)}{8D} L_{abs,0} \quad (2)$$

It should be noted that gravity induces sag in the tube when suspended in a horizontal position, reducing the amount of upward deflection. This sag is modeled by the deflection of a pinned-pinned Euler-Bernoulli beam exposed to a distributed load (tube weight per unit length).

$$y_{sag} = \frac{-5(\rho A g) L_{pin}^{\ 4}}{384 EI} \quad (3)$$

The length of tube exposed to gravitational sag (L_{pin}) is equal to the distance between the collars (4.27 m). The cross-sectional area A and the second moment of area I are both fixed by the absorber dimensions. Young's modulus E of the absorber steel decreases with temperature, which induces more sagging as the tube is heated. Summing thermal expansion and gravitational effects yields an analytic estimate of the vertical position of the absorber during heating.

Next, we describe the numerical approach. To avoid lengthwise temperature uniformity and an implicit parabolic assumption associated with the previous approach, the complete temperature field and assembly mesh are imported into a structural model solved with ANSYS 13.0 Workbench. As before, gravity must be applied as an inertial load on the model geometry to account for the inherent sagging of the tube.

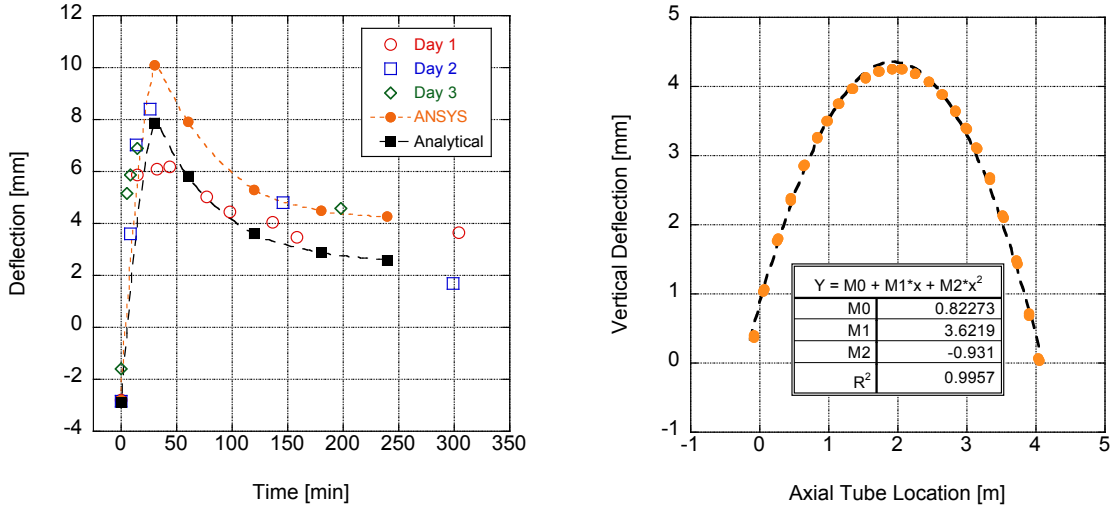

(a) (b)

Figure 3. (a) Vertical deflection of the empty absorber tube due to sun heating (measurement error ±1.5 mm). Zero deflection is defined as the ideal tube position without thermal expansion bending or gravitational sagging. (b) Axial tube profile along the top of the tube (Day 1) obtained from numerical modeling indicates that the deformed position can be represented well with a parabolic profile.

Solutions for the analytically and numerically obtained deflections are plotted in Figure 3a along with experimental data from three consecutive days of test with sun heating. The experimental data is measured as the distance between the external radii of the absorber and glass cover. The difference between the nominal separation (between the absorber and glass) and the measured gap defines the vertical deflection of the absorber. Eccentricity is accounted for by adjusting the initial position of the unheated absorber tube by the gravity sag. This correction value is then applied to each deflection measurement.

As seen in Figure 3a, the analytic and numerical deflection data agree to within 2.1 mm throughout the heating process. Prior to heating, both approaches predict initial sag (due to tube weight only) between -2.8 and -2.9 mm. Correcting the experimental data to this initial downward deflection yields reasonable agreement between the measurement and models, validating the two methodologies for an empty tube. The large deflection early in the heating process is attributed to the initial temperature disparity generated by the non-uniform heat flux. As the process continues, heat diffuses from the upper half of the absorber to the bottom half, reducing the temperature disparity and upward bending. Parallel to this, stiffness of the absorber decreases with temperature and generates more sagging. At the beginning of the next day's tests the tube has returned to its initial position indicating that the deflection was elastic (yield strength ~180 MPa at 200 °C).

While experimental data and the analytic approach only determine the vertical deflection of the absorber tube midpoint, the numerical method allows for the deflection to be solved along the entire length of the tube. This deflection profile is plotted in Figure 3b. The ends of the profile indicate the location of the collars. Also plotted is a second-order curve fit of the deflection, which matches the profile with a regression value of 0.996. Thus, the assumption of a parabolic profile in the analytic deflection model is adequate.

4. Filling Procedure

When filling receiver tubes with hot salt, the tubes are ideally preheated to a temperature comparable to the temperature of the liquid salt for two reasons. First, preheating avoids solidification of the salt on cold tube walls causing undesirable salt plugs. Second, minimizing the temperature difference between the salt and tube limits the amount of tube motion caused by a temperature differential across the height of the tube cross section. As shown above, for even moderate temperature differences on the order of 12 °C, significant motion in the tube can be observed.

When using impedance heat to warm the tubes, although the temperature may differ with axial position, the circumferential temperature gradient remains small and results in no significant vertical or lateral tube deformation. This is unlike that observed for heating the tube with the sun.

Receiver tube glass envelopes provide a dramatic reduction in heat loss along the tube length. Piping at the end of a row (eg. flex hoses) and couplings between neighboring receiver tubes typically have more heat loss per unit length than the evacuated receiver tubes despite added insulation. Therefore, when preheating with impedance heating, the axial tube center is typically hotter than the tube ends due to this heat loss. As a result, solidification initiates in the tube ends during a freeze event. If the wall temperatures in these connecting regions are matched to the liquid phase salt temperature, the resulting tube temperature at interior axial locations can be much higher than the salt temperature. As lower temperature salt moves down the length towards a higher temperature tube center, a temperature difference is established in the tube circumference and deformation is observed.

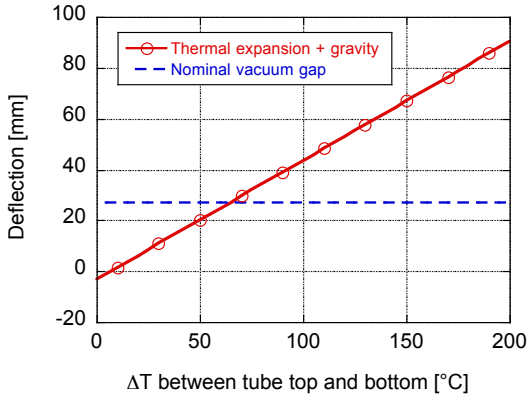

Figure 4. Combined deflection and gravity sag of an empty tube as a function of temperature difference between the top and bottom of the receiver tube (properties evaluated at 250 °C).

During an example filling procedure with a tube center temperature at ~300 °C and a liquid salt temperature of 260 °C, the observed rise in the receiver tube was as high as 16.6 mm as the salt was introduced to the tube. The tube then settled to 4.6 mm below the initial position as the liquid salt completely fills the tube cross section. The tube rise in position is commensurate with that expected for the 40 °C temperature difference between the tube center and liquid salt beginning to fill the bottom (see Figure 4). Once the tube is completely filled, the rise in position subsides as the circumferential temperature difference equilibrates. However, the resulting lower tube position is due to the added weight of the salt. From the distributed load beam deflection model in equation 3, the added liquid salt is expected to lower the tube position an additional 6.4 mm below that due to gravity sag alone and roughly agrees with the measured value. Thus, deflections caused by temperature differences between salt and tube during filling are also elastic when the deflection is within the confines of the glass envelope.

For large temperature differences between the tube and salt, the bottom wall can be drastically cooled as the salt starts to fill the receiver tube. Following the analytical approach of equation 3, a temperature difference between tube top and bottom on the order of 60 °C can result in deflections that might reach glass envelope. This also has been experienced and the authors have found the glass enclosure to be resilient to contact with the tube during filling. Regardless, matching of the salt temperature and the tube temperature all along the axial length is important to prevent breakage and maintain vacuum.

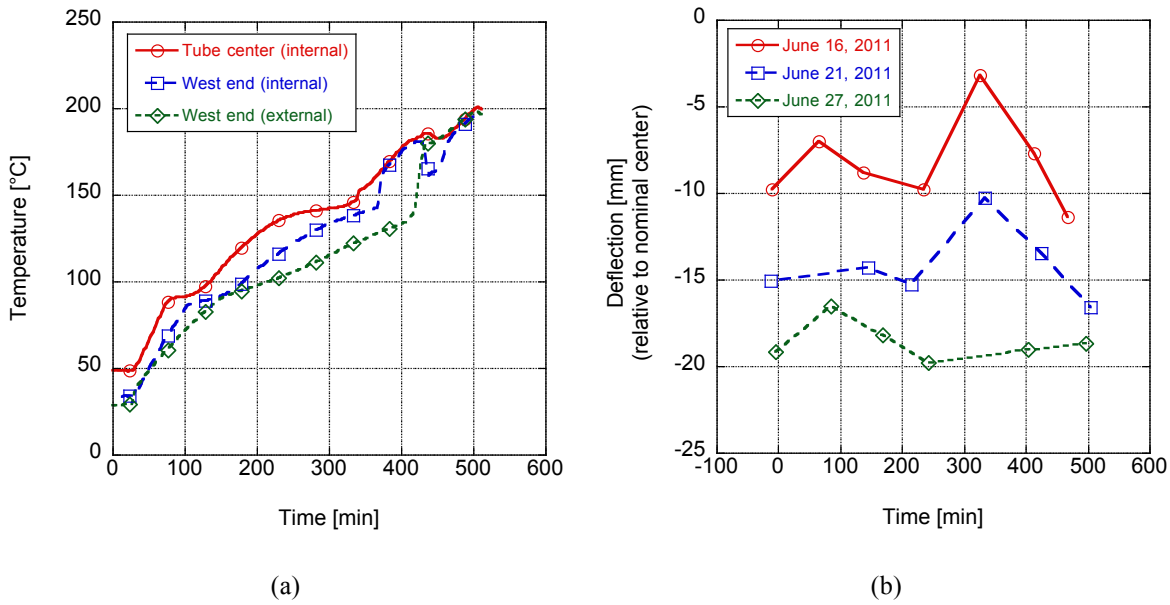

(a) (b)

Figure 5. (a) Internal temperatures as a function of time throughout the melting process of a single, salt-filled receiver tube for test on June 16, 2011. (b) Tube deflection through melt process for three test days (measurement error ±1.5 mm).

5. Freeze Thaw Cycles

Thermal cycling experiments to freeze and melt HITEC salt in a trough receiver tube using impedance heating have been performed following the mounting configuration of Figure 1. The tube was filled with salt and allowed to solidify while cooling to ambient temperature. For a single tube, 4.25 V was applied to the circuit, where 2.95 V was seen across the receiver tube resulting in approximately 715 W dissipated in heat. As the melting process began, temperatures and tube position were recorded using data acquisition and digital imagery. Figure 5a illustrates the ramping in temperature for the three internal thermocouples (see also Figure 1) for the first of three successive melt/freeze cycles. As shown in the figure, there is an initial sharp ramp in temperature as the salt volume increases in temperature. As the phase change process begins, this ramping slows as it approaches 150 °C (HITEC melt temperature = 142 °C). Once the salt has changed phase, another sharp increase in temperature is observed. The displacement of the tube during this June 16,

2011 experiment is indicated in Figure 5b. From the temperature curves, we can see that the salt has melted in around 5-6 hours from an initial temperature near ambient (~30 °C). If salt and tube were perfectly insulated, the heating time would decrease to around 2.8 hours from ambient condition through melt at the same power setting of 715 W.

Figure 5b illustrates the tube position as a function of time over three days of melt/freeze cycling. First we identify the starting position on June 16, 2011 near -10 mm. This initial deflection corresponds to the deflection due to gravity for a tube filled with salt. This value agrees well with a calculated deflection of -9.3 mm (using the analytical method above) assuming the salt is still warm and in the liquid phase. During the melt cycle, there is some obvious motion of the tube but once it reaches a fully melted condition, the tube position is near but slightly lower than what is observed at the start of the test. This additional decrease from the beginning of the test corresponds to softening of the metal and reduction in Young's Modulus with increasing temperature. An apparent decrease in position is observed during the freezing process such that the beginning of the next test starts at a lower initial position. Then a similar softening of the tube is observed as heating occurs resulting in a final position slightly lower than the initial position, as before. This process is repeated again during the third cycle and appears to have a progressive effect on the tube position. Possible reasons for this progressive lowering in tube position are currently being explored.

6. Intercepted Rays

In the event that tube deformation occurs, whether elastically during the heating process or plastically during successive phase-change thermal cycles, an estimate of the impact on the intercepted rays is necessary to determine the potential loss of energy. To characterize this loss in solar intercept, an LS-2 concentrator was selected as the baseline trough with a focal length of 1.49 m. For a 70 mm OD receiver tube centered in a 120 mm ID glass enclosure, the maximum deformation in any direction without compromising the glass-enclosed evacuated envelope is 2.5 cm. Assuming the mounting arms would limit the movement of the tube to only axial translation, the end points of the receiver tube are fixed for the purpose of quantifying the impact of deformation on solar intercept. The receiver tube was divided into 17 segments following an imposed parabolic deformation profile (as in Figure 3b) for several max deflections (0.5, 1 and 2.5 cm) at the midpoint. A sunshape by King [11] was used to define the solar energy source (at DNI = 1000 W/m^2) and SolTRACE [12] was used to model the intersection of 1 million rays to determine the total intercepted energy (see Figure 6).

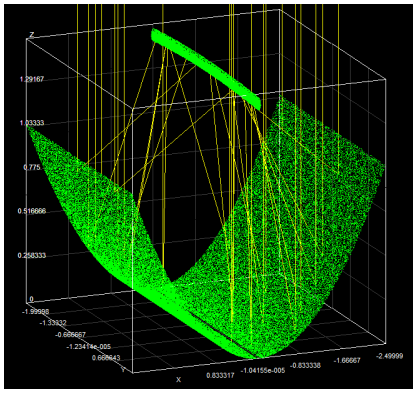

Figure 6. Sample illustration of intercepted rays on deformed tube.

Table 1 lists the percentage decrease in solar intercept for a deformed receiver tube (as described above) relative to an undeformed tube with the same concentrator and receiver conditions. Concentrator optics of both 3.0 and 5.4 mrad slope errors are provided which spans the range of likely total optical errors [13, 14]. Parallel and perpendicular deformation is referenced relative to the focal length direction. Long and short deformation indicates that the maximum parallel deformation position is longer or shorter than the focal length by the specified deflection. As shown by the percentages below, less than 7% reduction in solar intercept is expected for a tube that is deformed to a maximum position before reaching the glass envelope.

Slope error	Max deflection	Parallel deformation, long	Parallel deformation, short	Perpendicular deformation	Average decrease
3.0 mrad	0.5 cm	0.17%	0.24%	*	0.21%
	1 cm	0.46%	0.47%	*	0.47%
	2.5 cm	3.72%	3.66%	2.16%	3.18%
5.4 mrad	0.5 cm	0.16%	0.30%	0.44%	0.30%
	1 cm	1.11%	1.16%	1.21%	1.16%
	2.5 cm	6.39%	6.12%	6.41%	6.31%

* Within standard deviation of baseline case repeatability

Table 1. Percentage of decrease in solar intercept at several max deflections for 3.0 and 5.4 mrad slope errors (parallel and perpendicular directions are relative to the direction of the focal length).

Conclusions and Future Work

Trough receiver tubes have been shown to deform under loading as well as asymmetric heating conditions. In particular, when circumferential temperature gradients are established, tube deformation can be dramatic. In cases such as sun heating on an empty tube, impedance heating of an empty tube or during salt-filling procedures, tube deformation is observed as elastic. When salt fills the receiver tubes, permanent deformation can occur during cyclic melt/freeze cycles causing the tube to move away from the focal line. However, this motion appears to be modest and might result in a less than 7% loss in intercepted rays for even the most aggressive deformation. Future considerations include tube heating using concentrated sunlight and investigations into the phase-change process to determine the resulting impact on temperature gradients.

References

[1] Kearney D., Herrmann U., Nava P., Kelly B., Mahoney R., Pacheco J., Cable R., Potrovitza N., Blake D. and Price H., "Assessment of a molten salt heat transfer fluid in a parabolic trough solar field," *Journal of Solar Energy Engineering*, 125 (2003) 170-176.

[2] Falchetta M., Liberati G., Consoli D., Malloggi S., Mazzei D. and Crescenzi T., "Commissioning of the Archimede 5 MW molten salt parabolic trough solar plant," SolarPACES (2010) Perpignan, France, September 21-24, 2010.

[3] Bradshaw R. W., Cordaro J. G. and Siegel N. P., "Molten nitrate salt development for thermal energy storage in parabolic trough solar power systems," ASME Energy Sustainability (2009) San Francisco, CA, July 19-23, 2009.

[4] Raade J. W. and Padowitz D., "Development of molten salt heat transfer fluid with low melting point and high thermal stability," SolarPACES (2010) Perpignan, France, September 21-24, 2010.

[5] Kolb G. J., Ho C., Iverson B. D., Moss T. A. and Siegel N. P., "Freeze-thaw tests of trough receivers employing a molten salt working fluid," ASME Energy Sustainability (2010) Phoenix, AZ, USA, May 17-22, 2010.

[6] Iverson B. D., Broome S. T. and Siegel N. P., "Temperature dependent mechanical property testing of nitrate thermal storage salts," SolarPACES (2010) Perpignan, France, September 21-24, 2010.

[7] Iverson B. D., Cordaro J. G. and Kruizenga A. M., "Thermal property testing of nitrate thermal storage salts in the solid-phase," ASME Energy Sustainability (2011) Washington DC, USA, August 7-10, 2011.

[8] Macnification (2010) Vers. 1.7.1, Orbicule.

[9] Burkholder F. and Kutscher C., "Heat loss testing of Schott's 2008 PTR70 parabolic trough receiver," National Renewable Energy Laboratory (2009) NREL/TP-550-45633.

[10] ANSYS Workbench (2011) Vers. 13.0, ANSYS Inc.

[11] King D. L., "Beam quality and tracking accuracy evaluation of second-generation and Barstow production heliostats," Sandia National Laboratories (1982) SAND82-0181.

[12] Wendelin T. J., "SolTRACE: A new optical modeling tool for concentrating solar optics," International Solar Energy Conference (2003) Kohala Coast, HI, USA, March 15-18, 2003.
[13] Wendelin T. J., May K. and Gee R., "Video scanning Hartmann optical testing of state-of-the-art parabolic trough concentrators," ASME International Solar Energy Conference (2006) Denver, CO, July 2006.
[14] Kolb G. J. and Diver R. B., "Conceptual design of an advanced trough utilizing a molten salt working fluid," SolarPACES (2008) Las Vegas, NV, March 4-7, 2008.